Experimental and numerical serviceability assessment of a steel suspension footbridge

Eleonora Lai [a], Carmelo Gentile [b,*], Maria Gabriella Mulas [c]
[a] Politecnico di Milano, Department of Civil and Environmental Engineering (DICA), Piazza Leonardo da Vinci, 32, 20133 Milan, Italy
[b] Politecnico di Milano, Department of Architecture, Built environment and Construction engineering (DABC), Piazza Leonardo da Vinci, 32, 20133 Milan, Italy [c] Politecnico di Milano, Department of Civil and Environmental Engineering (DICA), Piazza Leonardo da Vinci, 32, 20133 Milan, Italy

The paper summarizes the main results of the serviceability assessment of a steel suspension footbridge, per-formed through dynamic testing and numerical simulations.
The experimental part of the study involved both operational modal testing and measurement of the structural response under the crossing of different groups of pedestrians. The footbridge exhibited quite complex dynamic characteristics (i.e. two couples of closely spaced modes and five modes in the frequency range 1.9–3.0 Hz) and the maximum accelerations induced by pedestrians and joggers turned out to be in the range of discomfort. An accurate FE model, based on the design drawings, was then developed and a general procedure is proposed to tackle the crucial issue of assigning the design tension forces to the suspension elements.
Since the comparison between numerical and experimental results generally shows a good agreement, the model is adopted to perform a numerical assessment of vibration serviceability according to the European guide-line HiVoSS. A minor shortcoming of HiVoSS and the unusual relevance of the 2nd harmonic of pedestrian-in-duced load are highlighted for the investigated footbridge.

Keywords:
Steel suspension footbridge
Human-induced vibration
FE modelling
Operational modal analysis
Vibration serviceability
2nd harmonic of pedestrian-induced load

1. Introduction

The design of recent footbridges is often inspired by aesthetics requirements for greater slenderness and results in longer spans, low ratio between permanent and live loads, and low damping [1]. This trend has been also favoured by the economic demand of efficiency, the increasing strength of materials and the relatively small service loads (as the structural design of footbridges is traditionally governed by the Ultimate Limit State, i.e. the load carrying capacity of the structural elements).

Consequently, the structural systems adopted on modern footbridges might exhibit dynamic behaviour marked by closely-spaced natural frequencies and/or frequencies very close to the values perceived by human beings [2–10], so that the design requires a greater care regarding vibration phenomena [11–12]. Well known examples of steel footbridges, that experienced serviceability problems associated to vibrations or required the design of tuned mass dampers to prevent this issue, include the Millennium bridge in London, UK [3], the Solférino bridge in Paris, France [4] and the Pedro e Inês footbridge in Coimbra, Portugal [7–8] (where the efficiency of the vibration control devices is also permanently assessed by a long-term dynamic monitoring system [13]).

Therefore, predicting the performance of footbridges to human-induced vibration has become a critical aspect of the structural design (see e.g. [1,7], [10–12]) so that different practical design methodologies have been developed, such as the French guideline Sétra [14] and the European guideline HiVoSS [15], that enable the designer to check the vibration serviceability of the footbridge for different pedestrian densities, based on a prediction of the maximum acceleration levels in vertical and lateral directions.

The paper presents the experimental and numerical vibration serviceability assessment of a slender steel suspension footbridge, overpassing the Serio River near Seriate, Italy. The investigated footbridge (Figs. 1–2) includes: (a) the deck, very slender and about 64.0 m long; (b) one main spatial system of suspension cables and hangers; (c) two steel frames supporting the suspension cables and the backstays.

Within the proof tests carried out before the bridge opening, dynamic tests were performed by the Laboratory of Vibration and Dynamic Monitoring of Structures (VibLab), Politecnico di Milano. Firstly, operational modal testing (with the excitation being mainly provided by micro-tremors and wind) was performed and 14 vibration modes were identified in the frequency range 0–10 Hz using different output-only techniques [16–17]: the frequency of the

Article history:
Received 3 August 2016
Received in revised form 29 December 2016
Accepted 1 January 2017
Available online xxxx

* Corresponding author.
E-mail addresses: eleonora.lai@polimi.it (E. Lai), carmelo.gentile@polimi.it (C. Gentile), mariagabriella.mulas@polimi.it (M.G. Mulas).

Published Journal Article available at: http://dx.doi.org/10.1016/j.jcsr.2017.01.005

Fig. 1. Footbridge crossing the Serio river (Seriate, Italy): (a) General view; (b) Underside view of the deck.

fundamental mode was 1.03 Hz and five modes turned out to fall in the frequency range 1.9–3.0 Hz. Subsequently, groups of volunteers (up to 32 adults) simulated normal walking and running along the deck. The human-induced vibrations were measured and the results clearly indicated that, especially in the vertical direction, the maximum acceleration values violate the human comfort serviceability conditions, when compared to limit acceleration targets present in references and design codes [14–15].

The numerical investigation relies on the development of a FE model, based on the as-built design data and implemented within the ANSYS [18] framework. A non-linear static analysis was performed to take into account the pre-tension forces in the suspension system, since the pre-tension in cables is crucial in determining the modal properties correctly. In order to assign the target (design) tensile forces to the suspension elements through fictitious thermal loads, a numerical procedure has been developed. The procedure is quite general and can be applied without any restriction to structural systems similar to the one at study.

A linear modal analysis was performed at the end of the non-linear static analysis, and the correlation between experimental and numerical modal parameters turned out to be fully satisfactory. It is worth underlining that no tuning procedures (see e.g. [2,5,19]) were adopted in the FE model of the footbridge, as in the typical situation at the design stage. Subsequently, the assessment of serviceability conditions was performed according to the European guideline HiVoSS [15].

After a brief description (Section 2) of the investigated footbridge, the paper describes the experimental procedures (Section 3) and the FE model development (Section 4). Subsequently, the numerical serviceability assessment is presented (Section 5) and conclusions are drawn.

2. The STEEL suspension footbridge

The investigated steel footbridge (Figs. 1–2) crosses the Serio River in the neighborhood of the town of Seriate (about 50 km far from Milan, Italy) and connects two cycle routes in the “Serio Park”.

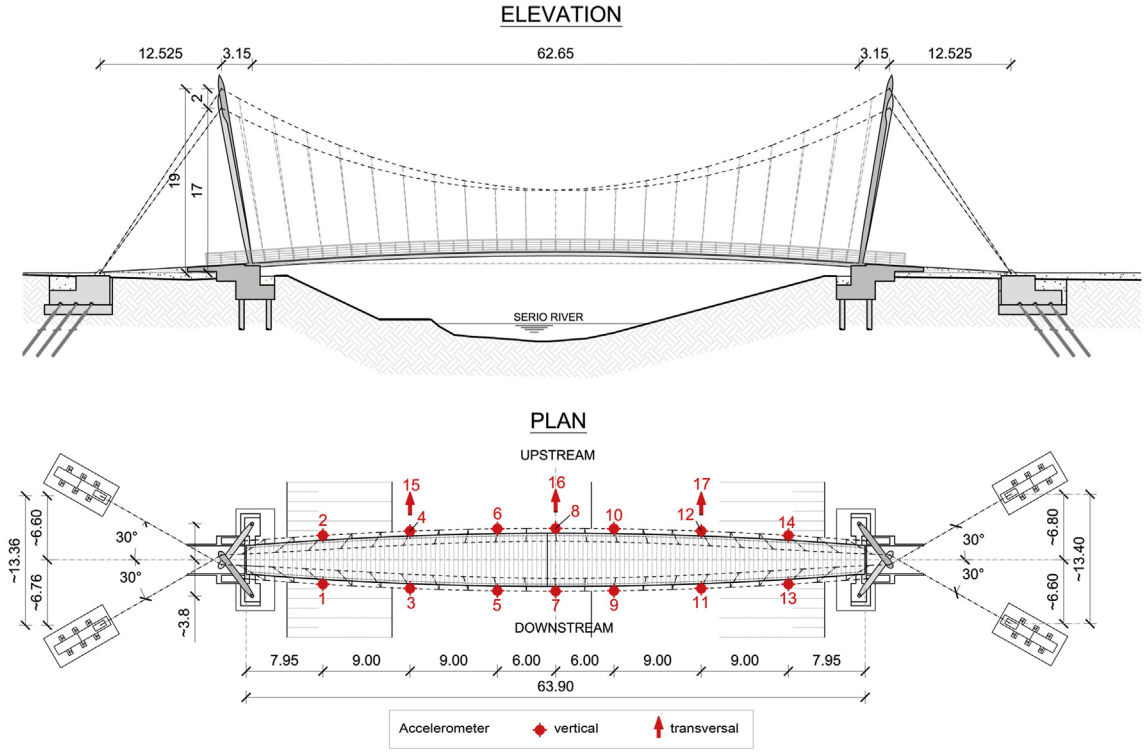

Fig. 2. Elevation and plan of the footbridge (dimensions in m). Accelerometer layout during the field tests.

The suspended deck, with an arch rise of 1.3 m, is 63.90 m long and its width varies between 2.5 m and 5.0 m. The deck consists of timber planks (providing the walking surface for the pedestrians), supported by a grid of steel stringers and floor beams (Figs. 1–2). The floor beams (Fig. 1b) belong to two classes: the main cross-beams, equally spaced at 3.0 m and characterized by a tapered cross-section, and the secondary transverse beams, with a standard European rolled-steel IPE 120 shape. The stringers include a couple of edge beams (European rolled-steel IPE 330 shapes) and a central girder with a hollow circular section ($Ø = 298.5$ mm). All the longitudinal beams are connected to the main cross-beams through bolted connections capable of restoring the continuity, whereas the connection between the secondary transverse beams and the edge beams allows the secondary beams to rotate around the edge beam axis. The ends of the main floor beams are crossed by a stabilizing cable (Fig. 1b), whose sliding in the longitudinal direction is permitted by the interposition of a polymeric layer between the contact surfaces. The deck is completed by a series of X-braces (Fig. 1b), providing stiffness in the horizontal plane.

The suspension system supporting the deck consists of:

- Four steel pylons, exhibiting a slight slope with respect to the vertical plane and arranged to constitute two A-shaped portal frames. The main suspension cables and the backstays are connected to the top of the pylons as it is shown in Figs. 1–2;
- Two main suspension cables, of 60 mm diameter, each supporting the deck through 21 hangers of 16 mm diameter, anchored at the ends of the main cross-beams;
- Four backstays, of 60 mm diameter, linking the pylons to the ground;
- Two lateral stabilizing cables, of 40 mm diameter and with opposing curvature (Fig. 1b).

As shown in Figs. 1–2, the suspension system is affected by a lack of symmetry about both the longitudinal vertical plane crossing the bridge axis and the transverse vertical plane crossing mid-span. About the longitudinal direction, the two hangers supporting the opposite ends of each cross-beam have different length and the main cables do not follow the same parabolic shape. About the transverse direction, each suspension cable has different anchoring position on the pylons at the two ends of the bridge (Fig. 1a).

During construction, all the cables were pre-tensioned. The design values of the tension were: (a) 425 kN for the backstays; (b) 500 kN for the stabilizing cables and (c) ranging between 10 and 17 kN for the hangers, subdivided into two sub-classes. The first sub-class includes the three couples of hangers close to the two deck ends, pre-tensioned at 13 kN (average value). The remaining hangers, placed in the central part of the bridge, are pre-tensioned at 15.5 kN (average value).

3. Experimental assessment of the dynamic behaviour

3.1. Experimental procedures

The dynamic characteristics of the footbridge were extensively investigated, right after its completion and before the opening, at the end of July 2012. More specifically, an ambient vibration test (AVT) was firstly developed with the objective of identifying the baseline dynamic characteristics (i.e. natural frequencies, mode shapes and damping ratios) of the structure. Subsequently, tests were performed with either walking or running pedestrians, to verify that the human-induced vertical and horizontal accelerations were limited to acceptable values. In the walking tests, the structural response associated to groups of 4, 8, 16 and 32 pedestrians crossing the bridge at a pace rate close to 2 Hz were measured, whereas the running test was performed with only 4 joggers.

The response of the footbridge was measured at 17 selected points in a single set-up (Fig. 2), using a 24-channel data acquisition system (24-bit resolution, 102 dB dynamic range and anti-aliasing filters) with uniaxial WR 731A piezoelectric accelerometers (Fig. 3). Each WR 731A sensor, capable to measure accelerations of ± 0.50 g with a nominal sensitivity of 10 V/g, was connected with a short cable (1 m) to a WR P31 power unit/amplifier providing the constant current needed to power the accelerometer's internal amplifier, signal amplification and selective filtering.

The acceleration responses were recorded with a sampling frequency of 200 Hz, which is fairly larger than that required for the considered footbridge, whose dominant natural frequencies are below 10 Hz. Hence, low pass filtering and decimation were applied to the data before using the identification tools: data were down-sampled to 25 Hz, so to have a Nyquist frequency of 12.5 Hz.

3.2. Operational modal analysis

As previously pointed out, the modal identification was performed by considering the accelerations mainly induced by micro-tremors and wind. Time series of 7200 s (corresponding to >7000 times the fundamental period of the bridge, quickly estimated through the frequency analysis of few minutes of data acquired in the first phase of AVT) were processed using different output-only identification algorithms in order to obtain estimates of natural frequencies, damping ratios and mode shapes. The modal parameters estimated by applying the Frequency Domain Decomposition (FDD) [16] and the data-driven Stochastic Subspace Identification (SSI-data) [17] techniques implemented in the commercial program ARTeMIS [20] will be presented in the following.

The lower singular values (SV) of the spectral matrix of the collected data using the FDD technique are shown in Fig. 4. It should be noticed that 14 relative maxima are clearly detected in the first SV line of Fig. 4: those peaks are generally well defined but two couples of closely spaced peaks (modes) are detected in the frequency range of 1.9–3.0 Hz. The estimates of the corresponding vibration mode components are shown in Fig. 5. The inspection of Fig. 5 highlights that: (a) the frequency of the fundamental mode is 1.03 Hz and the corresponding mode shapes involves anti-symmetric vertical bending of the deck; (b) almost all modes can be classified as dominant bending or dominant torsion, whereas only one mode, the fourth, exhibits coupling between vertical and transversal components; (c) five vibration modes turned out to fall in the critical frequency interval of 1.9–3.0 Hz.

The above dynamic characteristics were confirmed by applying different output-only identification algorithms. Table 1 summarizes the results obtained by applying the FDD and the SSI-data methods through: (a) the natural frequencies (f_{FDD}) identified by the FDD technique; (b) the average and the standard deviation values of the natural frequencies (f_{SSI}, σ_f) and modal damping ratios (ζ_{SSI}, σ_ζ) identified by the SSI method. Furthermore, Table 1 compares the estimates of corresponding mode shapes obtained by the two techniques through the Modal Assurance Criterion (MAC) [21].

The inspection of the values listed in Table 1 confirms that the natural frequencies estimated by the two different methods are practically coincident. A similar correspondence was found for most mode shapes (with the MAC value being larger than 0.98), except for the first torsion mode; for this mode, the MAC is about 0.88 and the FDD technique seems to provide a smoother estimation of the mode shape. It is further noticed (Table 1) that the modal damping ratio of 9 modes is lower than 1%; in addition, the scatter of the estimates seems quite limited (with the maximum standard deviation being 0.057%).

4. The finite element model of the footbridge

4.1. Ansys model

The FE model of the bridge (Fig. 6) is based on the as-built design data extracted from the blueprints. Within the ANSYS [18] framework, the steel stringers and transverse cross-beams of the deck, the pylons and the hangers are modeled with Timoshenko beam elements, with

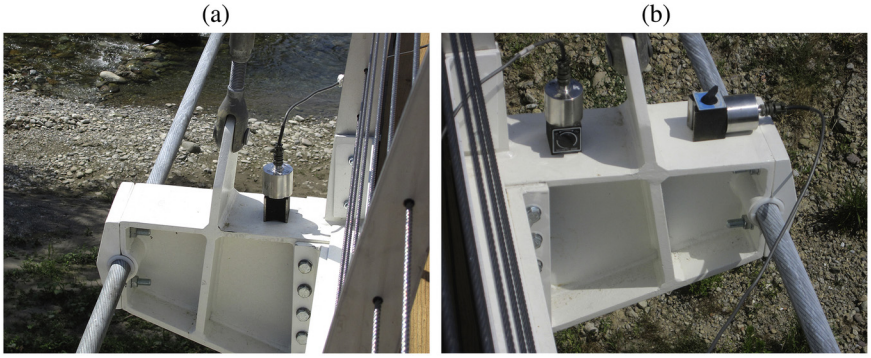

Fig. 3. Typical mounting of piezoelectric accelerometers on site.

6 degrees of freedom (DOFs) per node, named "BEAM 188" [18]. Cables and braces are represented by spar elements, transmitting only axial force and with 3 DOFs per node, named "LINK 180" [18]. The timber planks and the handrails of the deck are modeled as lumped masses applied on steel grid and their weight is included in the dead loads.

Boundary conditions are an idealization of the blueprint representations: (a) the transverse cross-beams at the opposite ends of the deck are constrained so that only the rotation of the deck in the longitudinal plane (i.e. around the transversal direction) is allowed; (b) similarly, only the rotation in the longitudinal plane is allowed at the base of each pylon; (c) both ends of backstays and main suspension cable are hinged. Furthermore, two different sets of constraint equations are adopted to simulate the connections between the secondary cross-beams and the stringers, and the sliding of the stabilizing cables, respectively. The former simulates an internal cylindrical hinge at the end of the cross beam, whereas the latter allows the stabilizing cables to slide in the longitudinal direction.

The overall bridge behaviour is affected by geometrical non-linearity, due to both the presence of cables and the geometry change associated to dead loads. For this reason, a preliminary non-linear static analysis was performed using the Newton-Raphson method [22]. Thus, loads are applied incrementally. Dead loads are applied first. Subsequently, the cable pre-tensions are imposed, element by element, through fictitious variations of temperature, determined according to a procedure, iterative in principle, herein proposed and described in the next sub-section. Once the model reproduces the design value of tension in cables (while matching the deformed geometry), a modal analysis is performed by using the stiffness matrix, associated to the deformed configuration of the footbridge under both the dead loads and the stress stiffening produced by pre-tension into suspension system.

4.2. The iterative procedure

Within each class of cables (backstays, hangers, stabilizing cables), the design pre-tension forces cannot be reproduced by uniform thermal loads. Element by element, the design value of tension N_d (i.e. the cable pre-stress) is obtained by applying an incremental load sequence, which includes firstly the dead loads $\boldsymbol{G}$ and subsequently a fictitious thermal load. The latter consists of an initial negative temperature $\boldsymbol{T}_{in}$, uniform for each class of elements, and of a thermal increment $\Delta\hat{\mathbf{T}}$, unknown in principle. Hence, the vector $\boldsymbol{N}_d$ collecting the design pre-tension forces can be seen as a function of $\boldsymbol{G}$, $\boldsymbol{T}_{in}$ and $\Delta\hat{\mathbf{T}}$:

$$\boldsymbol{N}_d = \boldsymbol{N}_d\left(\boldsymbol{G}'' + ''\boldsymbol{T}_{in}'' + ''\Delta\hat{\boldsymbol{T}}\right) \tag{1}$$

where the symbol "+" denotes the incremental application of each load contribution.

A trial-and-error method has been used to select the initial thermal load $\boldsymbol{T}_{in}$ (to be applied after the gravity load $\boldsymbol{G}$), that corresponds to a sufficiently close approximation of the design configuration. This initial configuration, due to $\boldsymbol{G}'' + ''\boldsymbol{T}_{in}$, is characterized by the design geometry of the deck (which is represented by the arch rise in the present case). However, the numerical values of the tension $\boldsymbol{N}_{0,d}$ associated to the initial configuration are generally different from $\boldsymbol{N}_d$. Consequently, it is necessary to introduce a further thermal load increment, in principle

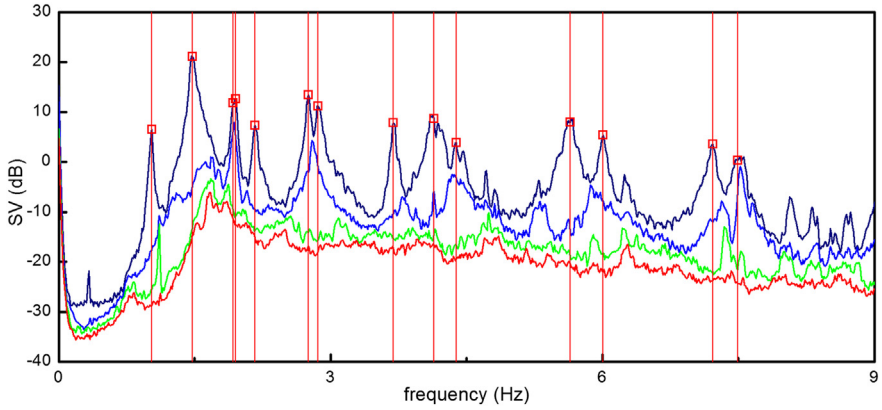

Fig. 4. Singular value lines (FDD) and identification of natural frequencies from the data measured on the bridge deck.

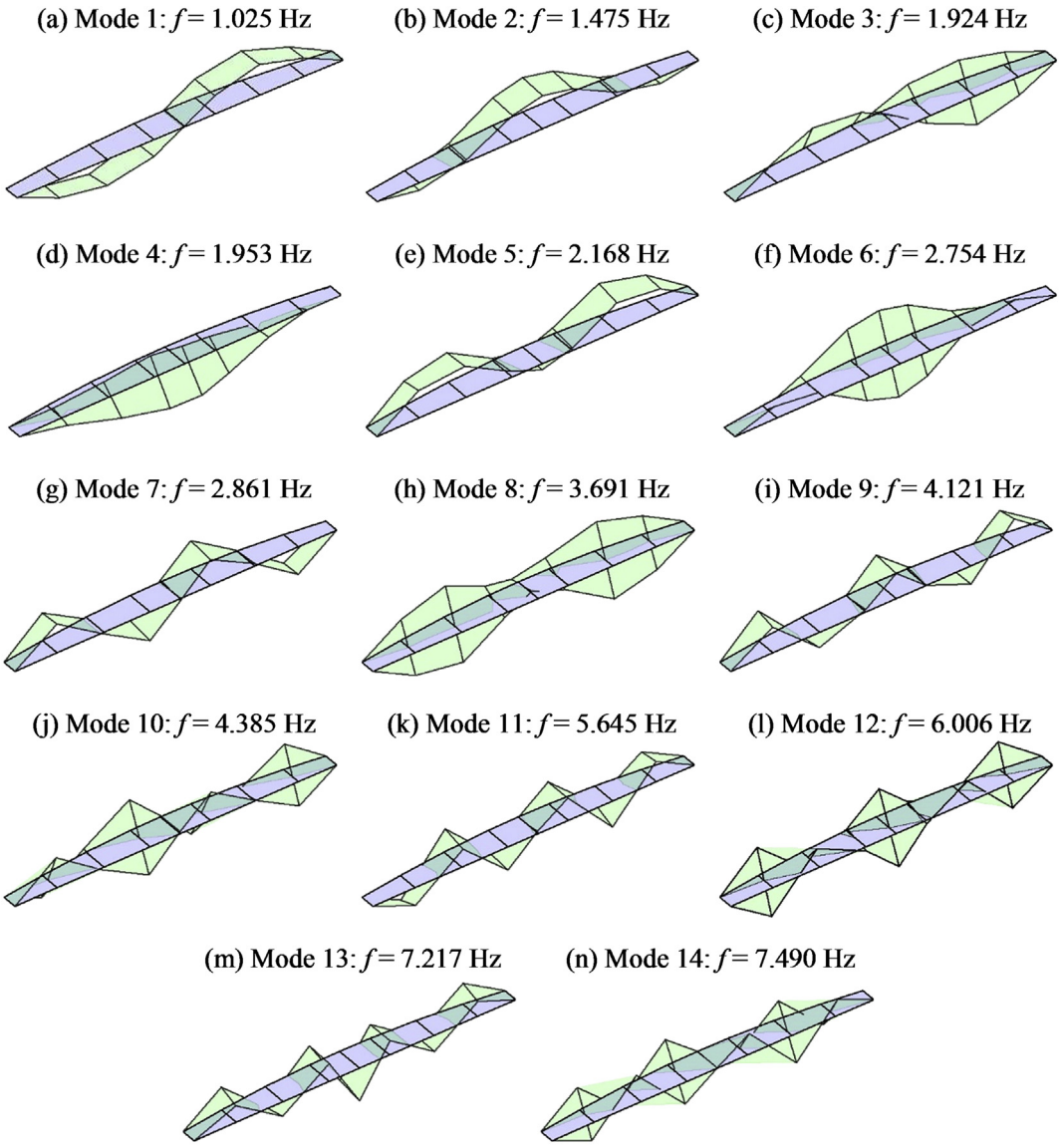

Fig. 5. FDD method: identified natural frequencies and mode shapes.

different for each cable element, which - added to the initial one $\boldsymbol{T}_{in}$ - provides the target design values $\boldsymbol{N}_d$. Under the assumption of linear behaviour of the bridge about the deformed initial configuration, obtained through the trial and error method, the vector $\boldsymbol{N}_d$ can be expressed as the sum of two terms:

$$\boldsymbol{N}_d = \boldsymbol{N}_{0,d}(\boldsymbol{G}'' + ''\boldsymbol{T}_{in}) + \Delta\boldsymbol{N}\left(\Delta\hat{\boldsymbol{T}}\right) \tag{2}$$

Table 1
Summary of the modal parameters identified by FDD and SSI-data methods.

Mode N.	Mode Shape	FDD	SSI-data				MAC
		f_{FDD} (Hz)	f_{SSI} (Hz)	σ_f (Hz)	ζ_{SSI} (%)	σ_ζ (%)	
1	Vertical/bending	1.025	1.014	0.002	0.75	0.016	0.997
2	Vertical/bending	1.475	1.474	0.004	1.58	0.034	1.000
3	Vertical/torsion	1.924	1.926	0.003	0.53	0.033	0.879
4	Vertical/Transv.	1.953	1.946	0.001	0.66	0.008	0.991
5	Vertical/bending	2.168	2.169	0.003	1.20	0.053	0.997
6	Vertical/torsion	2.754	2.756	0.001	0.74	0.003	0.997
7	Vertical/bending	2.861	2.860	0.001	1.32	0.004	0.997
8	Vertical/torsion	3.691	3.696	0.001	0.61	0.007	0.997
9	Vertical/bending	4.121	4.143	0.012	1.69	0.057	0.996
10	Vertical/torsion	4.385	4.408	0.003	1.11	0.029	0.995
11	Vertical/bending	5.645	5.636	0.008	0.94	0.011	0.995
12	Vertical/torsion	6.006	6.011	0.001	0.75	0.044	0.995
13	Vertical/bending	7.217	7.222	0.002	0.73	0.045	0.993
14	Vertical/torsion	7.490	7.488	0.003	0.78	0.009	0.988

As previously pointed out, in Eq. (2), the vector $\Delta\hat{\boldsymbol{T}}$ is unknown. However, it can be observed that, in the linearized case, an increment $\Delta\boldsymbol{N}(\Delta\boldsymbol{T})$ can be directly computed as the product of a proper matrix $[\boldsymbol{K}]$ by a vector of increments $\Delta\boldsymbol{T}(\neq\Delta\hat{\boldsymbol{T}})$:

$$\Delta\boldsymbol{N} = [\boldsymbol{K}]\Delta\boldsymbol{T} \tag{3}$$

The square matrix $[\boldsymbol{K}]$, having as dimensions the number n of elements to be prestressed ($n = 48$ in the present case), is derived similarly to a stiffness matrix: the column j represents the tension increment in each element due to a reference $\Delta T_j = +10\,^\circ$C in the *j-th* cable, with $\Delta T_i = 0$ if $i \neq j$. Therefore, the term K_{ij} represents the axial force increment in the *i-th* element due to $\Delta T_j = +10\,^\circ$C. A value $\Delta T_j = +10\,^\circ$C was chosen to produce a faster convergence and avoid problems with results too close to zero. Since the matrix $[\boldsymbol{K}]$ is derived for $\Delta T_j =$

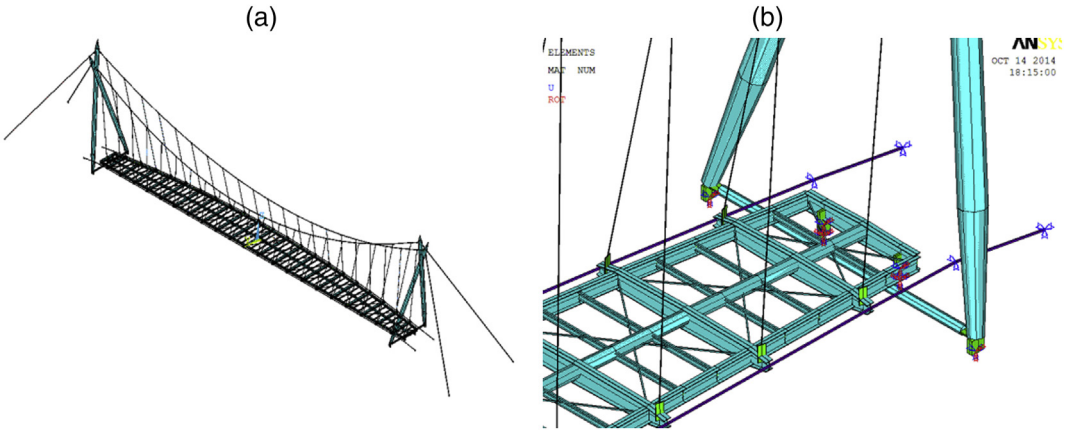

Fig. 6. Finite Element model of the footbridge: (a) overall view; (b) detail of steel grid.

+10 °C, the thermal increment to be inserted in (1) is computed as:

$$\Delta\hat{\boldsymbol{T}} = \frac{\Delta \boldsymbol{T}}{10\ ^\circ} \tag{4}$$

The non-linearity of the system affects the computation of the "stiffness-like" matrix [$\boldsymbol{K}$], whose columns $\boldsymbol{K_j}$ are given by the difference between:

(a) the tension $\boldsymbol{N}_{j,\Delta T}$ in a "perturbed" configuration, obtained from the initial configuration, by adding a $\Delta T_j = +10$ °C acting on the j-th element, and
(b) the tension $\boldsymbol{N}_{0,d}$ in each element due to the initial load configuration with gravity loads and the thermal loads uniform for each class of cables:

$$\boldsymbol{K}_j = \boldsymbol{N}_{j,\Delta T}\left(\boldsymbol{G}'' + ''\boldsymbol{T}_{in}\ '' + ''\Delta T_j\right) - \boldsymbol{N}_{0,d}(\boldsymbol{G}'' + ''\boldsymbol{T}_{in}) \tag{5}$$

Taking into account Eq. (3), Eq. (2) is rewritten as:

$$\boldsymbol{N}_{0,d}\,(\boldsymbol{G}'' + ''\boldsymbol{T}_{in}) + \ [\boldsymbol{K}]\Delta\boldsymbol{T} = \boldsymbol{N}_d \tag{6}$$

Moving $\boldsymbol{N}_{0,d}(\boldsymbol{G}'' + ''\boldsymbol{T}_{in})$ to the RHS of Eq. (6), an algebraic linear system of equations is obtained, having as unknown the vector $\Delta\boldsymbol{T}$ of thermal load increments to be applied in order to match the design values of tension:

$$[\boldsymbol{K}]\Delta\boldsymbol{T} = \boldsymbol{N}_d - \boldsymbol{N}_{0d}\,(\boldsymbol{G}'' + ''\boldsymbol{T}_{in}) = \Delta\boldsymbol{N}(\Delta\boldsymbol{T}) \tag{7}$$

or:

$$[\boldsymbol{K}]\Delta\boldsymbol{T} = \boldsymbol{q} \tag{8}$$

The solution of the system in (8) provides the values of the unknown vector $\Delta\boldsymbol{T}$:

$$\Delta\boldsymbol{T} = [\boldsymbol{K}]^{-1}\boldsymbol{q} \tag{9}$$

Introducing Eq. (4), the axial force in each element is then computed:

$$\hat{\boldsymbol{N}} = \boldsymbol{N}\left(\boldsymbol{G}'' + ''\boldsymbol{T}_{in}'' + ''\Delta\hat{\boldsymbol{T}}\right) \tag{10}$$

These tensions are compared with the design values through a residual term $\hat{\mathbf{R}}$ defined as:

$$\hat{\boldsymbol{R}} = \boldsymbol{N}_d - \hat{\boldsymbol{N}} \tag{11}$$

The norm of the vector Eq. (11), that would be zero in the ideal, linear case, gives a measure of the error in the values of pre-tension. If each component of $\hat{\mathbf{R}}$ is within a pre-selected tolerance, the corresponding

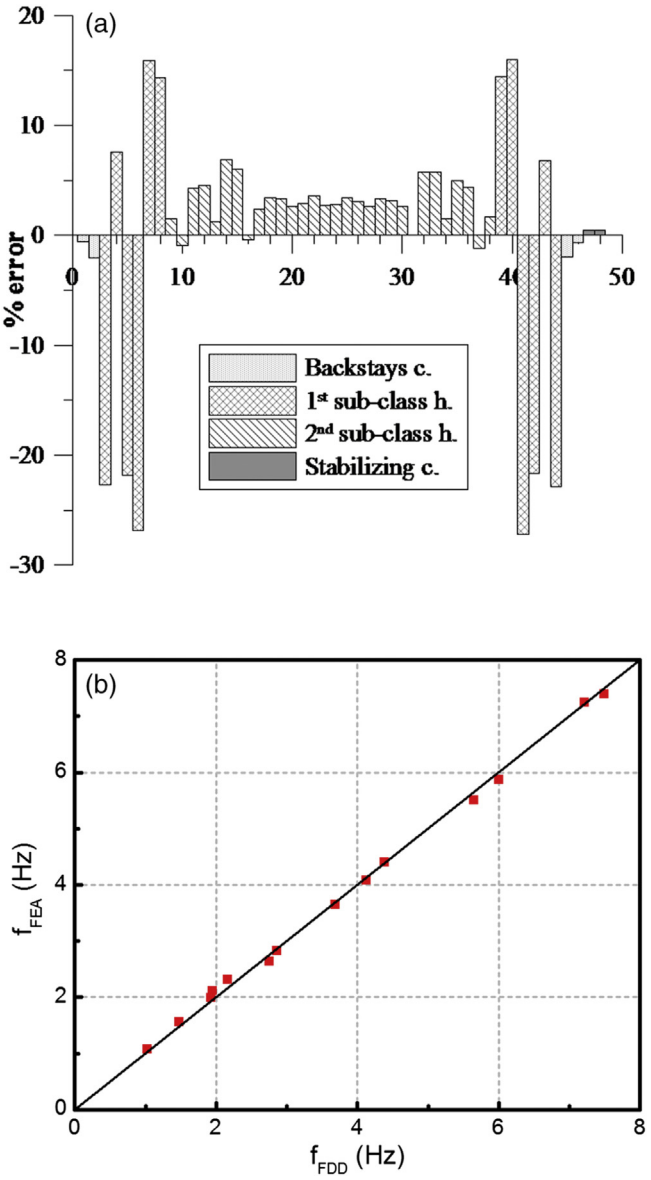

Fig. 7. Results of numerical analyses: (a) percentage error on the cable pre-stress tension; (b) correlation between numerical (f_{FEA}) and experimental (f_{FDD}) frequencies.

load configuration is assumed for the subsequent analyses:

$$\textit{Final load configuration} = \boldsymbol{G}'' + ''T_{in}'' + ''\Delta\hat{\boldsymbol{T}} \tag{12}$$

In the opposite case, an iteration process can be started, where the residual term in Eq. (11) at iteration k becomes the new constant term of the linear system Eq. (8) at the subsequent iteration $k + 1$:

$$\boldsymbol{q}^{(k+1)} = \boldsymbol{R}^{(k)} \tag{13}$$

Eqs. (8) to (11) are repeated until convergence is achieved within the prefixed tolerance. At each iteration k a further thermal load increment $\Delta\hat{\mathbf{T}}^{k}$ is added to the load configuration. The final load configuration is obtained by summing up the contributions of the m iterations performed:

$$\textit{Final load configuration} = \boldsymbol{G}'' + ''T_{in}'' + ''\Delta\hat{\boldsymbol{T}}^{(k=1)}'' + ''\Delta\hat{\boldsymbol{T}}^{(k=2)}'' + ''\ldots'' + ''\Delta\hat{\boldsymbol{T}}^{(k=m)} \tag{14}$$

Different tolerances have been prescribed for backstays and stabilizing cables (10 kN) and for hangers (1 kN), reflecting the order of magnitude of pre-tension in cables and hangers (order of hundreds against tens). The iterative procedure has shown a different

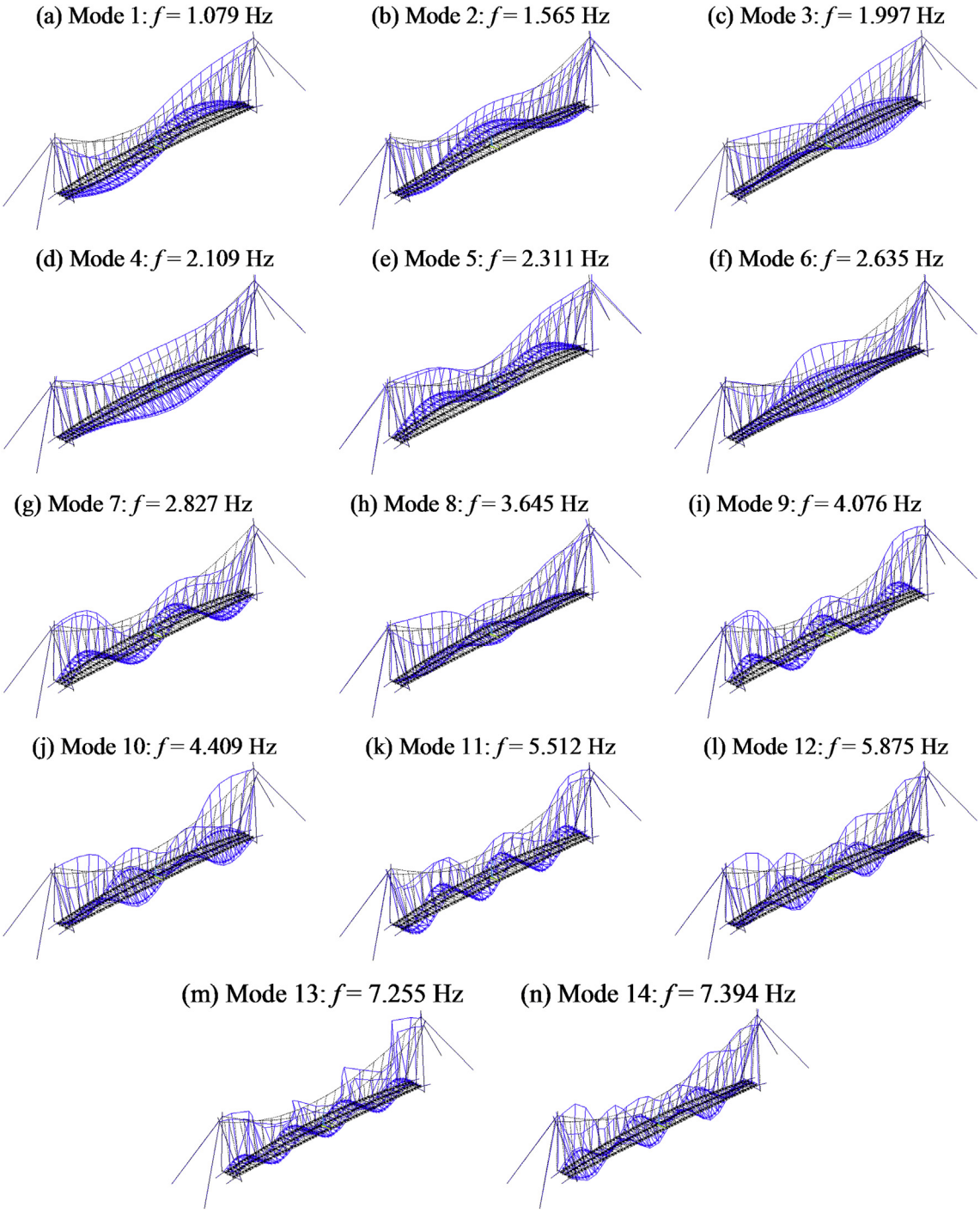

Fig. 8. FE model of the bridge: mode shapes and natural frequencies.

Table 2
Comparison between experimental (FDD) and numerical results.

Mode	Frequency (Hz)		ε (%)	MAC
	Experimental	Numerical		
1	1.025	1.079	5.22	0.995
2	1.475	1.565	6.07	0.994
3	1.924	1.997	3.77	0.908
4	1.953	2.109	7.99	0.842
5	2.168	2.311	6.58	0.984
6	2.754	2.635	−4.33	0.975
7	2.861	2.827	−1.17	0.996
8	3.691	3.645	−1.24	0.957
9	4.121	4.076	−1.10	0.988
10	4.385	4.409	0.55	0.982
11	5.645	5.512	−2.36	0.958
12	6.006	5.875	−2.18	0.982
13	7.217	7.255	0.52	0.976
14	7.490	7.394	−1.28	0.983

Table 3
Maximum recorded accelerations due to walking.

Position	Vertical acceleration (m/s^2)			
	4 pedestrians	8 pedestrians	16 pedestrians	32 pedestrians
A1	1.04	1.67	1.49	1.54
A2	0.91	1.56	1.33	1.64
A3	1.22	1.77	1.44	1.77
A4	1.03	1.78	1.27	1.42
A5	0.81	0.78	0.97	1.32
A6	0.68	0.70	0.78	1.17
A7	0.93	0.83	0.88	1.26
A8	0.74	0.89	0.96	1.47
A9	0.75	0.92	0.76	1.22
A10	0.67	0.87	0.86	1.10
A11	1.08	1.79	1.46	1.52
A12	1.20	1.97	1.11	1.85
A13	0.87	1.77	1.11	1.83
A14	0.96	1.88	1.30	2.07
Position	Horizontal acceleration (m/s^2)			
	4 pedestrians	8 pedestrians	16 pedestrians	32 pedestrians
A15	0.28	0.33	0.39	0.34
A16	0.25	0.27	0.28	0.41
A17	0.25	0.34	0.26	0.36

performance of the convergence criterion. One iteration was enough to reduce the error within the tolerance for the stabilizing cables, the backstays cables and the second sub-class of hangers but not for the first sub-class of hangers.

Fig. 7a shows the distribution of the percentage error on the pre-tension in cables, normalized to the design values, at the end of the first iteration; a positive value denotes a numerical overestimation of the design tension. The graph in Fig. 7a presents the values in the same order the cables are encountered moving from one bridge end to the other. The last two values refer to the stabilizing cables. It is easy to recognize a pattern on the error tied to the position of the cable: the error for cables in the first sub-class has the same pattern at the two ends, with positive and negative values balancing to produce an average value of about 5%.

The error shown in Fig. 7a increases with the number of iterations, possibly due to the significant non-linearity of the system. To overcome this drawback, the "stiffness-like matrix" [***K***], here assumed to be constant during the iteration process, should be updated at each iteration, following a Newton-Raphson scheme to make null the residual term. The updating of [***K***] would result in a severe computational burden since the determination of each column involves a nonlinear analysis. However, the configuration corresponding to the results of the first iteration was deemed to be acceptable due to the close match between identified and numerical dynamic properties (Fig. 7b), as it will be discussed in the next sub-section.

4.3. Comparison between numerical and experimental dynamic properties

The validation of the numerical model is based on the comparison of the dynamic properties with the experimental estimates obtained through the Frequency Domain Decomposition (FDD) method. The mode shapes of the numerical model are shown in Fig. 8, for the natural modes corresponding to the experimentally identified modes (Fig. 5). For each mode both the numerical (f_{FEA}) and the experimental (f_{FDD}) frequencies are provided. The correlation in terms of natural

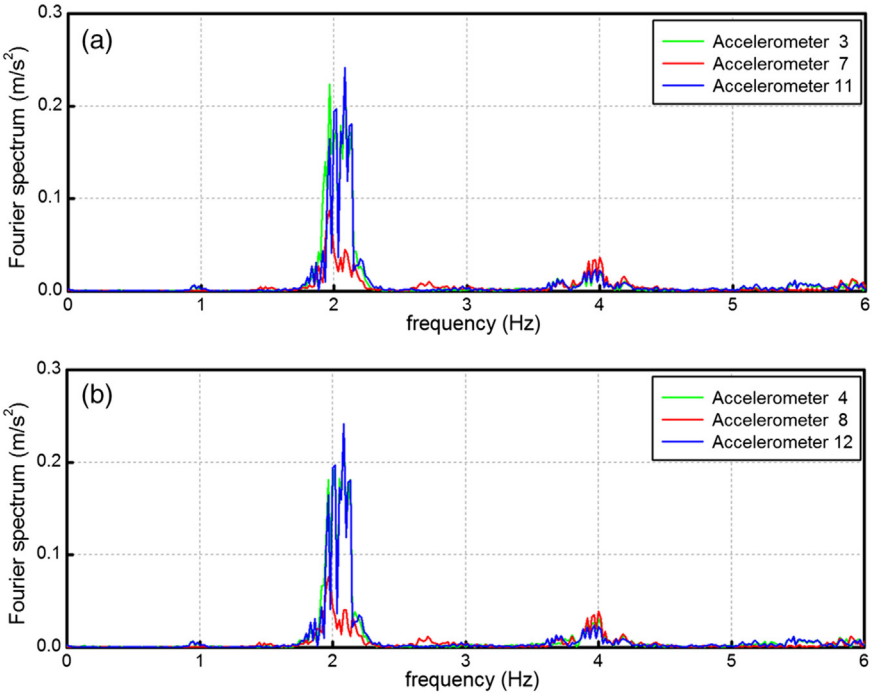

Fig. 9. Fourier spectrum of sample vertical accelerations (8 pedestrians walking) measured: (a) on downstream side; (b) on upstream side.

Table 4
Loading scenarios and maximum recorded accelerations.

No. of pedestrians	Walking	Running	Position	Max. vert. acc. (m/s^2)	Position	Max. horiz. acc. (m/s^2)
4	✓		A3	1.22	A15	0.28
8	✓		A12	1.97	A17	0.34
16	✓		A1	1.49	A15	0.39
32	✓		A14	2.07	A16	0.41
4		✓	A5	4.80	A15	1.09

Table 5
Pedestrian traffic classes and density [15].

Traffic class	Density (pedestrian/m^2)	Description
TC1	$15P/(B \times L)$	Very weak
TC2	0.2 P/m^2	Weak
TC3	0.5 P/m^2	Dense
TC4	1.0 P/m^2	Very dense
TC5	1.5 P/m^2	Exceptionally dense

frequencies is summarized in Fig. 7b, whose results fully justifies the choice not to refine further the bridge load configuration. Table 2 quantifies the value of ε, percentage frequency error between numerical and experimental values:

$$\varepsilon\,[\%] = 100 \times (f_{FEA} - f_{FDD})/f_{FDD} \quad (15)$$

The MAC values, listed in the last column of the same Table 2, confirms the high consistency between the numerical and experimental mode shapes.

Based on the correlation between numerical and experimentally identified modal parameters, two remarks can be drawn:

1. As shown in Fig. 9, the natural frequencies of the numerical model provide a fairly good approximation of the actual footbridge frequencies. Indeed the frequency deviations exhibit a peculiar trend, that is characterized by larger discrepancies - ranging between 3.77% and 7.99% - for the lower six modes and very limited deviations - from −2.36% to 0.55% - for the remaining 8 modes. This trend is conceivably due to the poor prior knowledge that is available about the effects of non-structural elements, such as the timber planks and the handrails, and the stiffness of the supports. Also the error in the tension of first-sub-class hangers could have played a role. In addition, it is worth recalling that the footbridge was tested at the end of July 2012, so that also the temperature might have affected the tension forces in the cable and consequently the modal frequencies;
2. The correlation between the numerical and experimental mode shapes is generally excellent, as it can be easily verified from both the direct inspection of the vibration modes illustrated in Figs. 5 (experimental) and 8 (FE model) and the MAC values (last column of Table 2) very close to one (i.e. between 0.957 and 995) for 12 modes. Only the mode shapes associated to the closely spaced frequencies of 1.92 and 1.95 Hz (modes 3 and 4) exhibit a MAC of 0.908 and 0.843, respectively.

5. Vibration serviceability due to walking

5.1. Assessment of pedestrian effects: experimental results

The analysis of the identified frequencies and mode shapes, summarized in Fig. 5 and Table 1, highlighted the existence of five vibration modes in the frequency range of 1.9–3.0 Hz, the same of the dynamic loading induced by pedestrians either walking (3th, 4th and 5th mode) or running (6th and 7th mode). Hence, resonance effects could appear in the bridge response.

To assess the levels of vibration, various loading scenarios were defined and simulated on site with the help of groups of volunteers, who were asked to walk both along the longitudinal bridge axis and in an eccentric position with respect to the bridge axis. Table 3 shows, for each measurement point (see Fig. 2), the maximum values of the vertical and horizontal acceleration due to walking. Table 4 summarizes, for each loading scenarios, the maximum values of vertical and horizontal acceleration due to both walking and running.

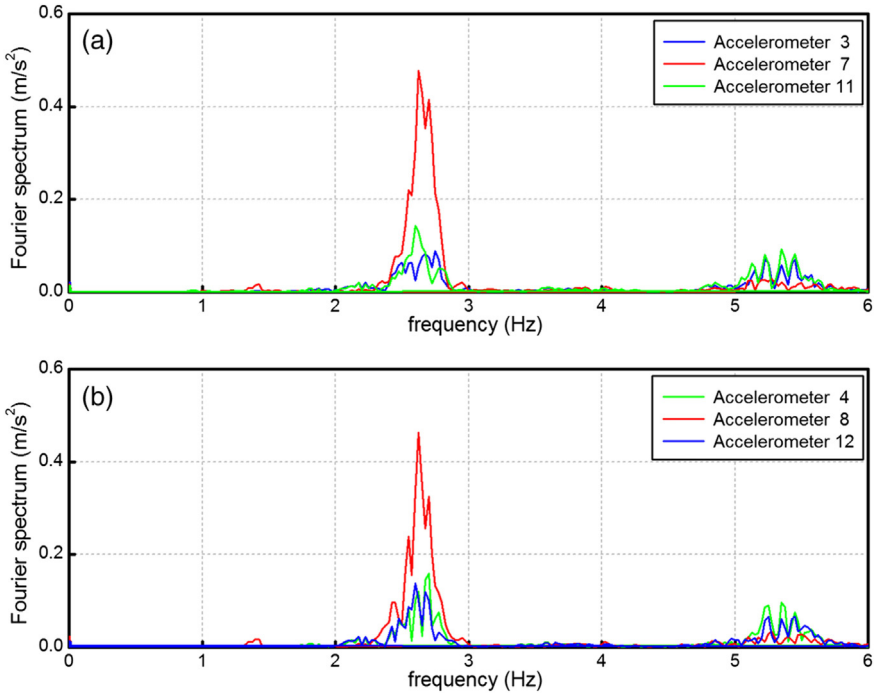

Fig. 10. Fourier spectrum of sample vertical accelerations (4 pedestrians running) measured: (a) on downstream side; (b) on upstream side.

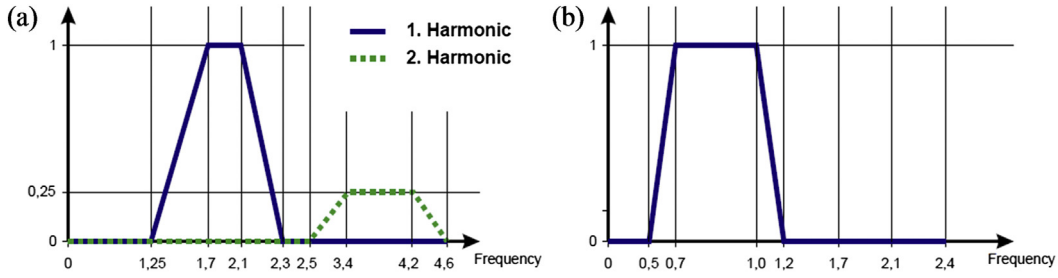

Fig. 11. Reduction factor ψ: (a) vertical and longitudinal load, (b) lateral load (from [15]).

The inspection of the acceleration values summarized in Tables 3 and 4 shows that:

- even for the walking of small groups of pedestrians (4–8 pedestrians), the recorded accelerations are relatively high in the vertical direction;
- increasing the number of pedestrians from 4 to 8 to 16–32 does not produce a significant increase of the maximum vertical acceleration, due to the difficulty of ensuring synchronization among pedestrians as their number increases;
- the maximum accelerations due to pedestrians walking are recorded approximately at quarter span, where the 3rd and 5th mode shapes attain their maximum displacements;
- the maximum acceleration induced by 4 running joggers is extremely high (0.48 g);
- the maximum accelerations due to running are recorded at central sections of bridge deck. This pattern is opposite to that induced by walking pedestrians, because runners excite the 6th and 7th mode, whose shape shows a maximum displacement field in the area close to half-span;
- the level of vibration associated to the horizontal/transversal direction, although not negligible, is significantly lower than that observed in the vertical direction, where the maximum acceleration values significantly exceed the limit values recommended in [14–15].

It is worth mentioning that eccentric transits generate higher accelerations due to the torsion and lateral behaviour of the 3rd, 4th and 6th mode shapes.

The Fourier spectrum of the accelerations recorded at mid-span and quarter spans is shown in Fig. 9 for the case of 8 pedestrians walking, and in Fig. 10 for the 4 pedestrians running, respectively. Figs. 9a and 10a refer to downstream side, whereas Figs. 9b and 10b refer to the opposite upstream side. The spectra confirm that modes 3–5 (Fig. 5c–e) and modes 6–7 (Fig. 5f–g) are responsible of the footbridge behaviour under walking and running scenarios, respectively. In fact, modes 3 and 5 exhibit the largest modal deflections approximately at quarter spans, where the largest spectral amplification is detected in Fig. 9a and b. Moreover, the spectral amplification at mid-span becomes important in Fig. 10a and b, highlighting the role of mode 6.

The Fourier spectrum of Fig. 9 shows two frequency intervals where the peak values are found. The first one, with largest values, is centred about 2 Hz, and the second one, with lower but not negligible values, is centred about 4 Hz. Hence, the effect of the second harmonic of the pedestrian-induced load is clearly detected. A similar pattern, representative of the same effect, is found in Fig. 10, where the intervals are centred about 2.75 and 5.50 Hz, i.e. the frequency values associated to running-induced loads.

5.2. HiVoSS guideline

The numerical assessment of the serviceability conditions of the footbridge follows the guideline HiVoSS [15], developed within the context of an European research project named SYNPEX [23]. For the sake of completeness, the main features of the guideline are summarized in the following.

As well documented in the literature [1], the load associated to the single pedestrian can be considered as the sum of Fourier harmonic components. Nevertheless, it is worth mentioning that: (a) either groups of pedestrians or a crowd can cross a footbridge; (b) the corresponding load is affected by both inter-subject variability (i.e., each pedestrian has his own weight, step frequency, step length and arrival time) and intra-subject variability (i.e., the pedestrians tend to adjust their motion on that of nearby people, and possibly synchronizing with them).

The pedestrian load, mainly of random nature, is approximated in the HiVoSS guideline with a deterministic, uniformly distributed, harmonic load $p(t)$ [N/m^2] representing an equivalent pedestrian stream:

$$p(t) = P \cdot \cos(2\pi f_s t) \cdot n' \cdot \psi \tag{16}$$

In Eq. (16), $P \cdot \cos(2\pi f_s t)$ is the harmonic load due to a single pedestrian. P is the component of the force due to a single pedestrian, taking into account the dynamic load factor, i.e. the coefficient of the Fourier series ($P = 280$ N for vertical load, $P = 140$ N for longitudinal load and $P = 35$ N for lateral load). The walking step frequency f_s is assumed equal to any of the footbridge natural frequencies under consideration. The reduction coefficient ψ takes into account the probability that the footfall frequency approaches the critical range of natural frequencies under consideration. The parameter n' is the equivalent number of perfectly synchronised pedestrians, on the loaded surface S. A definition of n' is given for the two cases of: (a) sparse crowd, when each pedestrian can move freely on the footbridge and (b) dense crowd, when free motion is no longer possible and a higher degree of synchronization can be found among pedestrians.

Adopting a concept typical of performance-based design in the bridge assessment, the designer evaluate the expected traffic conditions, and associate comfort requirements to them. Five conditions,

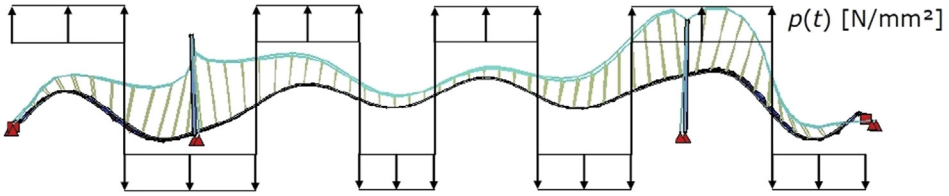

Fig. 12. Application of a harmonic load according to mode shape (from [15]).

Table 6
Comfort classes with common acceleration ranges [15].

Comfort class	Degree of comfort	Vertical a_{lim}	Lateral a_{lim}
CL1	Maximum	<0.5 m/s^2	<0.1 m/s^2
CL2	Medium	0.5–1.0 m/s^2	0.1–0.3 m/s^2
CL3	Minimum	1.0–2.5 m/s^2	0.3–0.8 m/s^2
CL4	Unacceptable discomfort	>2.5 m/s^2	>0.8 m/s^2

described in Table 5, range from a very weak traffic (TC1) to a very dense one (TC5) and encompass persistent, transient and accidental or exceptional design situations. A typical example of the last one is the bridge inauguration. The equivalent number of pedestrians n' depends on the traffic class, as a function of the structural damping ratio ξ, the loaded surface S and the number of pedestrians n on the surface ($n = S \cdot d$):

- Sparse crowd classes TC1 to TC3 (density $d < 1.0$ P/m^2). In the first TC1 class only 15 pedestrians are moving on the whole area B × L of the footbridge.

$$n\prime = \frac{10.8\sqrt{\xi \cdot n}}{S} \qquad \left[\frac{1}{\mathrm{m}^2}\right] \tag{17}$$

- Dense crowd classes TC4 to TC5 (density $d \geq 1.0$ P/m^2).

$$n\prime = \frac{1.85\sqrt{n}}{S} \qquad \left[\frac{1}{\mathrm{m}^2}\right] \tag{18}$$

Since harmonic load models describe the pedestrian excitation, the critical range of the footbridge natural frequencies f corresponds to the range of the first harmonic of pedestrian load, whose structural effects are prevailing on the subsequent ones [15]:

- for vertical and longitudinal vibrations: 1.25 Hz ≤ f ≤ 2.3 Hz;
- for lateral vibrations, the range of frequencies is roughly halved, since the right and left foot transmit opposite forces: 0.5 Hz ≤ f ≤ 1.2 Hz.

The second harmonic of pedestrian loads might excite to resonance footbridges with natural frequencies in the range 2.5 Hz ≤ f ≤ 4.6 Hz. In this case, the critical frequency range for vertical and longitudinal vibrations expands to 1.25 Hz ≤ f ≤ 4.6 Hz. Lateral vibrations are not affected by the second harmonic of pedestrian loads. The value of the reduction coefficient ψ for the first and second harmonic of the pedestrian load and for vertical and longitudinal load is depicted in Fig. 11a. Fig. 11b shows the value for lateral load. The direction of the harmonic load is the same of the half-waves characterizing the mode shapes associated to the natural frequency considered in the dynamic analysis (Fig. 12).

The assessment of the serviceability conditions is necessary if any of the footbridge natural frequencies falls in the critical range and is performed through a dynamic harmonic analysis of the footbridge. Four comfort classes, in a descending order from a maximum comfort (CL1) to an unacceptable discomfort (CL4), are devised in terms of either vertical or lateral acceleration (Table 6). Since the footbridge is located in a country park, where the probability to find a "dense traffic" is very small, only two design conditions were considered: traffic class TC1 (very weak traffic), associated to a comfort class CL1, and traffic class TC2 (weak traffic), associated to a comfort class CL2. Vibration serviceability criteria are satisfied if the computed values of the acceleration response do not exceed the limits corresponding to the comfort class.

5.3. Assessment of pedestrian effects: numerical results

The footbridge shows 10 natural frequencies in the critical bandwidth (Table 2). The frequency of 1st mode is in the critical range for lateral vibration. The frequencies of modes 2–9 fall in the range that is critical for vertical and longitudinal vibrations. Moreover, starting from the fifth mode, the 2nd harmonic of pedestrians load has to be considered. For each frequency, and for each traffic class considered, a dynamic analysis was performed with ANSYS, in which a harmonic load acts on the whole deck, with a direction coherent with the one of corresponding mode shape, and an excitation frequency in resonance with the one of bridge.

In each harmonic analysis, the experimentally identified damping ratios (Table 1) were adopted for both defining the equivalent number of pedestrians n' and evaluating the numerical responses. The numerical results in terms of maximum accelerations were evaluated in three points belonging to the cross sections at half-span and quarter-spans. More specifically, two points are placed at the base of handrails, as in the experimental tests, and the third one is on the longitudinal axis of the footbridge deck: Fig. 13 shows the points position and their numbering in the FE model.

The bridge mode shapes exhibit bending or torsion behaviour, except for the 4th mode (Figs. 5d and 8d), characterized by a displacement field also in the transverse/horizontal plane. For each vertical mode, the significant response parameter is the amplitude of the vertical

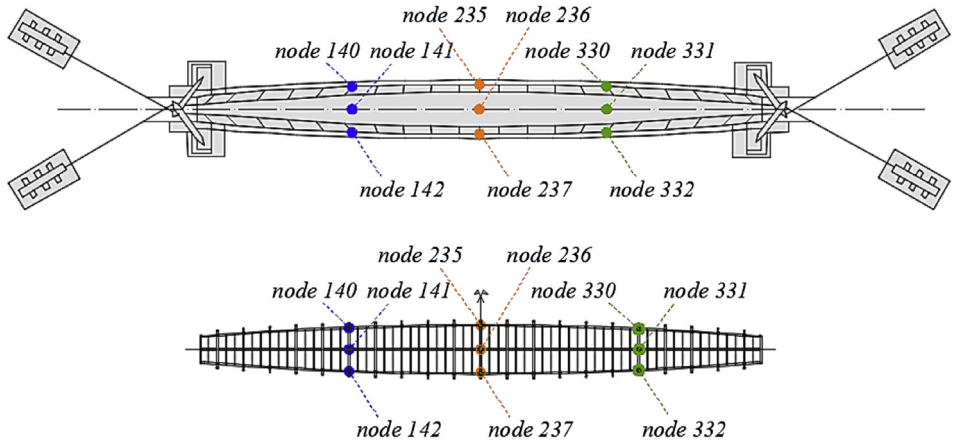

Fig. 13. Cross sections and numbering of points in the numerical assessment based on HiVoSS Guideline [15].

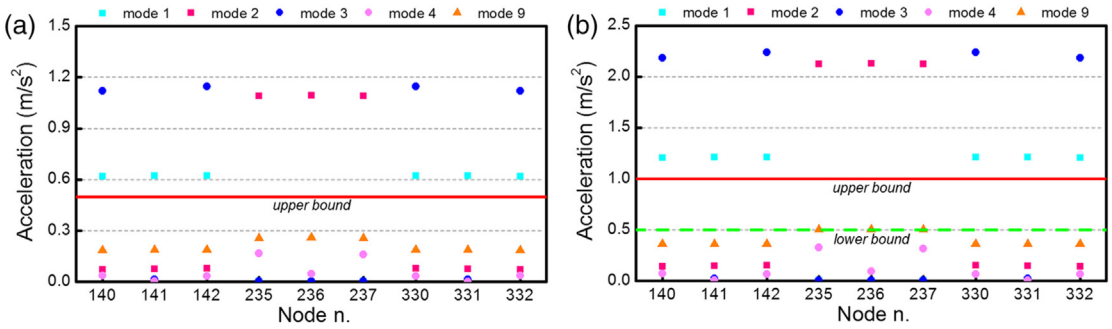

Fig. 14. Serviceability assessment for vertical vibration: (a) traffic class TC1; (b) traffic class TC2.

acceleration due to the related harmonic load, at the selected nodes and for each mode within the critical range. The 5th mode has not been considered, as its frequency (2.31 Hz) in the numerical model is associated to a null reduction coefficient ψ (Fig. 11a). Lateral accelerations are considered for the harmonic load tuned to the 4th mode.

It is worth mentioning that the peak acceleration associated to modes 6–8 and 10 turned out to be almost negligible (i.e. 2–3 orders lower than the overall maximum vertical acceleration computed for both traffic classes). Hence, only the results related to modes 1–4 and 9 are illustrated in Fig. 14a and b, which refer to traffic class TC1 and TC2, respectively. Fig. 15a and b show the analogous results for the lateral vibration related to the 4th mode. In Figs. 14b and 15b the dashed line represent the lower limit of acceleration for class TC2. The graph area is ideally subdivided in three sub-region, each corresponding to one of the cross-section at study (nodes 140–142; 235–237; 330–332). The central node of each section is associated to the central result in each sub-zone of the graph.

Fig. 14a and b highlight the same pattern of results for the first three modes, with the vertical accelerations significantly exceeding the upper bound (denoted with a thick solid line). The maximum values, more than twice the upper bounds in Table 6, are found in the three nodes of midspan for the 2nd mode (Fig. 8b) and, with similar but slightly larger values, in the two end nodes of the sections at quarter spans for the 3rd mode (Fig. 8c).

It is further noticed that, as it has to be expected from the relevant mode shapes (Fig. 5a–c and Fig. 8a–c): (a) the accelerations associated to the 1st mode exceed the limit (of about 20%) at quarter span cross-sections, whereas are practically zero at midspan; (b) the same acceleration, associated to the 2nd mode, is experienced by the three nodes at midspan; (c) the two nodes reaching the extreme values associated to the 3rd mode (torsion) are placed on the opposite sides of the two cross-sections. Consequently, the out-of-bound response of the midspan section is due only to the 2nd mode, with practically null values related to 1st and 3rd mode. For the quarter-span sections, the accelerations due to the 1st mode are uniform on the three nodes while those due to the 3rd mode are almost null along the bridge axis and reach the extreme values at the two ends.

The role of the 4th and 9th mode deserves further comments:

a) Fig. 14 highlights that the response due to the 9th mode (Fig. 8i) is within the limit for class TC1 and on the lower comfort limit for class TC2. In addition, the accelerations due to this mode are practically uniform over each cross-section, with values slightly larger at midspan than at quarter spans;
b) The vertical acceleration related to the 4th mode (Fig. 8d) is within the limit for class TC1 and at the lower bound for class TC2 (Fig. 14). However, lateral vibration related to this mode exceeds the limit for both TC1 and TC2 (Fig. 15);
c) When the excitation frequency exceeds the value of the 4th mode, the second harmonic of pedestrians loads comes into play. The significant response due to both 4th and 9th mode indicates that for this particular footbridge also this harmonic must be considered.

Due to the difference in the loading scenarios, the accelerations recorded during the experimental tests cannot be directly compared with the numerical results obtained by applying the HiVoSS guideline. However, the order of magnitude of numerical and experimental values is the same. In addition, the Fourier spectrum in Fig. 9, extracted from the results in terms of vertical acceleration of dynamic tests, has a frequency content concentrated between 1.8 and 2.2 Hz, where modes 3–5 of the footbridge (Fig. 5c–e) fall.

However, two main discrepancies are found between numerical and experimental results, related to the contributions of the 1st and 5th mode. The former appears to be significant in the numerical analyses, but not in the experimental results (Figs. 9 and 10). The harmonic load tuned with the latter does not produce any critical acceleration in the numerical simulation, since its reduction factor is equal to zero. Thus, the relevant contribution of the 5th mode, as it appears in the

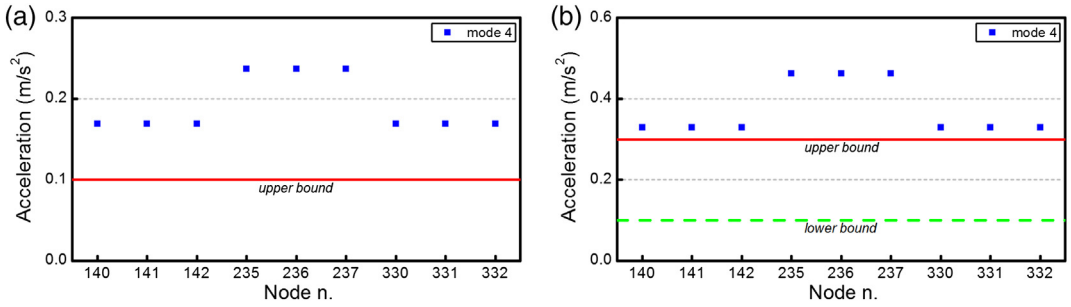

Fig. 15. Serviceability assessment for lateral vibration: (a) traffic class TC1; (b) traffic class TC2.

experimental data, is neglected when the numerical procedure of HiVoSS guideline is applied.

6. Conclusions

The results of the serviceability assessment of a lively steel suspension footbridge are presented in the paper. The assessment is based on both an experimental campaign including operational modal testing and walking and running test, and numerical analyses on an accurate FE model developed in ANSYS. The numerical assessment complies with a current code of practice, the HiVoSS guideline [15], for two traffic classes, very weak and weak (TC1, TC2), respectively associated to maximum CL1 and medium CL2 comfort classes. The following main conclusions can be drawn from the experimental campaign:

(a) Within the frequency range 0–10 Hz, 14 vibration modes were successfully identified in operational conditions, using the Frequency Domain Decomposition [16] and the data driven Stochastic Subspace Identification [17] techniques and a good agreement was generally found between the two methods in terms of both natural frequencies and mode shapes.
(b) The identification of natural frequencies and mode shapes provided the necessary data for highlighting serviceability issues of the structure.
(c) Three vibration modes turned out to fall in the frequency interval of 1.9–2.2 Hz, critical for walking activities, whereas two other modes were identified in the interval 2.5–3.0 Hz, critical for running activities. Moreover, non-negligible vibrations have been detected due to the load second harmonic of pedestrians, either walking or running.
(d) The accelerations measured under walking and running scenarios exceed comfort values. The frequency content of the signals turned out to be dominated by the contribution of the relevant modes in the two intervals described in point (b).

The FE model, based on as-built drawings, has successfully matched the experimentally identified modal parameters of the footbridge. Since the global dynamic characteristics of the investigated suspension bridge are highly affected by the tensile forces in the cables and no field data were collected on the cable tensions, it is worth noting that the match in terms of modal parameters has been found only when the design values of cable pre-tension have been simulated through fictitious temperature variations, applied properly to each cable. Thus, the numerical procedure herein proposed (Section 4.2) for the computation of the fictitious thermal loads, has been a key point in this work.

The numerical serviceability assessment according to the HiVoSS guideline has shown that the accelerations due to the harmonic loads tuned to the first 4 modes exceed the comfort limits in both traffic classes considered. Even though the loading scenarios are different, the results are in good agreement with the experimental outcomes, with two main differences related to the role of the 1st and 5th mode. The former affects the numerical results but not the experimental outcome, whereas the latter fades in the numerical analyses due to the null value of the reduction factor ψ in the relevant frequency range (2.3–2.5 Hz).

Finally, in the implementation of HiVoSS guideline [15], the 2nd harmonic of pedestrian load has to be considered for frequencies exceeding 2.5 Hz. Among the modes in the related frequency range, one (i.e., the 9th) is associated to significant values of acceleration. Hence, the role of the second harmonic of the load is highlighted and this result seems quite significant, as it is explicitly stated in [15] that no case of bridges significantly excited by this harmonic was reported yet.

References

[1] S. Živanović, A. Pavic, P. Reynolds, Vibration serviceability of footbridges under human-induced excitation: a literature review, J. Sound Vib. 279 (1–2) (2005) 1–74.
[2] J.M.W. Brownjohn, Vibration characteristics of a suspension footbridge, J. Sound Vib. 202 (1) (1997) 29–46.
[3] P. Dallard, T. Fitzpatrick, A. Flint, A. Low, R. Smith, M. Willford, M. Roche, The London Millennium footbridge: pedestrian-induced lateral vibration, J. Bridg. Eng. 6 (2001) 412–417.
[4] P. Dziuba, G. Grillaud, O. Flamand, S. Sanquier, Y. Tetard, La passerelle Solférino. Comportement dynamique, Bull. Ouvrages Metal. 1 (2001) 34–57.
[5] S. Živanović, A. Pavic, P. Reynolds, Modal testing and FE model tuning of a lively footbridge structure, Eng. Struct. 28 (2006) 857–868.
[6] J.G.S. da Silva, P.C.G. da S. Vellasco, S.A.L. de Andrade, L.R.O. de Lima, F.P. Figueiredo, Vibration analysis of footbridges due to vertical human loads, Comput. Struct. 85 (21—22) (2007) 1693–1703.
[7] E. Caetano, Á. Cunha, F. Magalhães, C. Moutinho, Studies for controlling human-in-duced vibration of the Pedro e Inês footbridge, Portugal. Part 1: assessment of dy-namic behaviour, Eng. Struct. 32 (2010) 1069–1081.
[8] E. Caetano, Á. Cunha, F. Magalhães, C. Moutinho, Studies for controlling human-in-duced vibration of the Pedro e Inês footbridge, Portugal. Part 2: implementation of tuned mass dampers, Eng. Struct. 32 (2010) 1082–1091.
[9] C. Moutinho, Á. Cunha, E. Caetano, Analysis and control of vibrations in a stress-rib-bon footbridge, Struct. Control Hlth. 18 (6) (2011) 619–634.
[10] R. Salgado, J.M. Branco, P.J.S. Cruz, G. Ayala, Serviceability assessment of the Góis footbridge using vibration monitoring, Case Studies Non-destruct. Test Eva. 2 (2014) 71–76.
[11] G. Piccardo, F. Tubino, Simplified procedures for vibration serviceability analysis of footbridges subjected to realistic walking loads, Comput. Struct. 87 (13–14) (2009) 890–903.
[12] K. Van Nimmen, G. Lombaert, G. De Roeck, P. Van den Broeck, Vibration serviceabil-ity of footbridges: evaluation of the current codes of practice, Eng. Struct. 59 (2014) 448–461.
[13] W.H. Hu, C. Moutinho, E. Caetano, F. Magalhães, Á. Cunha, Continuous dynamic monitoring of a lively footbridge for serviceability assessment and damage detec-tion, Mech. Syst. Signal Process. 33 (2012) 38–55.
[14] Sétra, Evaluation du comportement vibratoire des passerelles piétonnes sous l'action des piétons, 2006.
[15] Research Fund for Coal and Steel, HiVoSS: Design of Footbridges, Guideline EN03, 2008.
[16] R. Brincker, L.M. Zhang, P. Andersen, Modal identification from output-only systems using frequency domain decomposition, Smart Mater. Struct. 10 (2001) 441–445.
[17] P. Van Overschee, B. De Moor, Subspace Identification for Linear Systems: Theory, Implementation, Applications, Kluwer, Boston/London/Dordrecht, 1996.
[18] ANSYS, Online Manuals Release 5.5, http://mostreal.sk/html/guide_55/GBooktoc.html2015.
[19] C. Gentile, N. Gallino, Ambient vibration testing and structural evaluation of an his-toric suspension footbridge, Adv. Eng. Softw. 39 (2008) 356–366.
[20] SVS, ARTeMIS Extractor, Release 5 (3) (2011) 2012http://www.svibs.com.
[21] R.J. Allemang, D.L. Brown, Correlation coefficient for modal vector analysis, Proceed-ings of the 1st Int. Modal Analysis Conf. (IMAC-I), Orlando, FL, USA, 1983.
[22] T. Belytschko, W.K. Liu, B. Moran, Nonlinear Finite Elements for Continua and StructuresJohn Wiley & Sons Ltd 2000.
[23] European Commission, Research Fund for Coal and Steel. SYNPEX: Advanced Load Models for Synchronous Pedestrian Excitation and Optimised Design Guidelines for Steel Footbridges, Final Report, 2008.